Early Detection of Thermoacoustic Combustion Instability Using a Methodology Combining Complex Networks and Machine Learning

Tsubasa Kobayashi, Shogo Murayama, Takayoshi Hachijo, and Hiroshi Gotoda*
Department of Mechanical Engineering, Tokyo University of Science, 6-3-1 Niijuku, Katsushika-ku, Tokyo 125-8585, Japan

(Received 25 January 2019; revised manuscript received 2 May 2019; published 14 June 2019)

We undertake an experimental study on the early detection of combustion-driven thermoacoustic instability using a method combining complex networks and machine learning. The probability distribution of the transition patterns in ordinal partition transition networks significantly captures the subtle changes in the combustion state during a transition from combustion noise with a low amplitude to thermoacoustic combustion instability with a high amplitude. A feature space consisting of the principal component plane estimated from the probability distribution of the transition patterns, which is obtained by a support vector machine, allows us to detect a precursor of thermoacoustic combustion instability.

DOI: 10.1103/PhysRevApplied.11.064034

I. INTRODUCTION

Self-sustained thermoacoustic instability resulting from mutual interference between the resonant acoustics and heat release in a confined system produces a rich variety of highly nonlinear dynamic behavior. It provides extremely promising prospects for developing new engine systems [1,2], but the strong vibration of the system during thermoacoustic instability leads to unacceptable structural damage to land-based gas-turbine and propulsion systems. Therefore, online detection methodologies to prevent the onset of potentially destructive combustion-driven thermoacoustic instability are a currently important objective in applied physics and related fields of thermal fluid science, including the characterization of combustion dynamics from a stable state to a well-developed limit cycle via intermittent thermoacoustic instability. Details of the onset mechanisms on thermoacoustic combustion instability in various turbulent combustors from laboratory to industrial levels [3–5] have recently been studied. The suppression of thermoacoustic combustion instability has newly been addressed by Biwa *et al.* [6].

The growing availability of complex networks has given rise to a platform for obtaining a comprehensive understanding of the topological complexity in real-world systems [7]. Complex networks have recently spilled out into the areas of combustion physics and engineering with high expectations for the novel characterization of complex combustion dynamics and the development of up-to-date detectors of thermoacoustic combustion instability [5]. Two important network properties, the scale-free nature [8–10] and the small-world nature [10,11], have been found in the network connectivity constructed from pressure fluctuations in thermoacoustic combustion systems, showing the importance of natural visibility graphs for probing a precursor of thermoacoustic combustion instability [9] and lean blowout [10]. More recently, spatiotemporal dynamics of flow velocity fluctuations during thermoacoustic combustion instability have been extensively studied using recurrence networks and turbulence networks [12]. Nonlinear dynamics of thermoacoustic combustion instability have been successfully elucidated within the framework of graph theory, but the physical understanding and the development of detectors of thermoacoustic combustion instability based on a complex-network approach remain challenging problems. Machine-learning technology has played a key role in bringing major changes to all scientific disciplines and possesses significant potential for establishing new combustion control systems. Our primary interest in this study is to explore the possibility of a complex-networks/machine-learning-based approach for the early detection of thermoacoustic combustion instability. The purpose of this study is to build a new online early-detection methodology that integrates complex networks and machine learning to avoid the onset of combustion-driven thermoacoustic instability. As an important case study of thermoacoustic combustion instability, we focus on the combustion dynamics in a swirl-stabilized-type turbulent combustor [12]. The mutual coupling between pressure and heat-release-rate fluctuations has a significant impact on the onset of thermoacoustic combustion instability [4]. On this basis, we adopt ordinal partition transition networks [13,14] considering the interaction pattern

*gotoda@rs.tus.ac.jp

between multivariate time series for pressure fluctuations and OH* chemiluminescence emission intensity fluctuations, where OH* is the excited OH radical. The standard support vector machine (SVM) [15,16], which is a class of machine learning to recognize patterns, is a binary classifier predicting the boundaries of classes and has received considerable attention in data science for the past few decades [17]. To detect a precursor of thermoacoustic combustion instability, we adopt the SVM for the principal component plane estimated from the probability distribution of the transition patterns in ordinal partition transition networks by principal component analysis (PCA). This paper is organized into four parts. We briefly explain the experimental system in Sec. II and the mathematical framework of the analytical methods in Sec. III. The results and discussion are presented in Sec. IV and we give a summary in Sec. V.

II. EXPERIMENTS

A schematic diagram of our experimental system is shown in Fig. 1. The combustion rig is the same as that used in a recent study [12] except for a swirler. The swirler we used in this study, which contains an injector with eight holes of diameter 0.6 mm, is placed at the inlet of the combustion chamber to act as a flame holder. The combustor is equipped with the quartz windows to visualize the combustion dynamics. A methane-main air premixture with a swirl number of 0.70 [12] is supplied to the combustion chamber at a volume flow rate (mean axial flow velocity at the inlet of the combustion chamber) of 152.4 L/min (6.0 m/s). The initial equivalence ratio of the fuel/main air premixture ϕ without issuing steady secondary air is varied from 0.65 to 0.84 to focus on the significant transition from combustion noise with a low amplitude to thermoacoustic combustion instability with a high amplitude. The OH* chemiluminescence emission intensity is assumed to represent the heat release rate from the flame. In this study, we simultaneously measure the pressure fluctuations p' and OH* chemiluminescence emission intensity fluctuations I'_{OH^*}. p' is measured by a water-cooled pressure transducer (JTEKT Products, PD104K-10kPa) mounted 20 mm from its inlet on the wall of the combustion chamber. I'_{OH^*} is measured by both a photomultiplier (Hamamatsu Photonics, H10722-210) and a high-speed camera (Photron, FASTCAM SA-Z) with an image intensifier (Hamamatsu Photonics, C9548-03). An OH band-pass filter (ASAHI SPECTRA Co., UZ0310) with a bandwidth of $\pm$ 2 nm centered at a wavelength of $\lambda = 310$ nm is set in front of the photomultiplier and the high-speed camera lens. The actual size of each image obtained by the high-speed camera is 100 $\times$ 100 mm with a resolution of 512 $\times$ 512 pixels. The sampling frequency of p' and I'_{OH^*} is 6 kHz. Note that the high-speed camera images are used to obtain the synchronization index [18].

III. MATHEMATICAL FRAMEWORK OF ANALYTICAL METHODS

We here briefly describe the central ideas behind the analytical methods employed in this study. The dynamic behavior of thermoacoustic combustion instability has been proactively studied from the viewpoint of synchronization theory [19–22]. Our recent study [18] has shown that a new index derived by a dynamical systems/synchronization-based approach, namely, the synchronization index, enables us to extract the driving region of thermoacoustic combustion instability. In this study, we first adopt the synchronization index S_I, defined as the product of the joint probability of recurrence plots J_r [23] and the phase synchronization parameter r_{pq}, to study the significant change in the dynamics from combustion noise to thermoacoustic combustion instability with increasing equivalence ratio:

$$S_I = J_r r_{pq}, \tag{1}$$

$$J_r = \frac{M - R_r}{1 - R_r}. \tag{2}$$

Here, J_r is the joint probability of recurrence plots [23]; R_r $(= \sum_{m,n} R_{m,n}/N^2)$ is the recurrence rate, $M = [(1/N^2)\sum_{m,n}^{N} J_{m,n}]/R_r, J_{m,n} = \Theta[\epsilon - ||\mathbf{p}(t_m) - \mathbf{p}(t_n)||]\Theta[\epsilon - ||\mathbf{W}_{\mathbf{OH}^*}(t_m) - \mathbf{W}_{\mathbf{OH}^*}(t_n)||]$, Θ is the Heaviside function, $\mathbf{p}(t) = \{p'(t), p'(t+\tau), \ldots, p'[t+(D-1)\tau]\}$, $\mathbf{W}_{\mathbf{OH}^*}(t) = \{W'_{\mathrm{OH}^*}(t), W'_{\mathrm{OH}^*}(t+\tau), \ldots, W'_{\mathrm{OH}^*}[t+(D-1)\tau]\}$, and D is the dimension of the phase space. The second-order

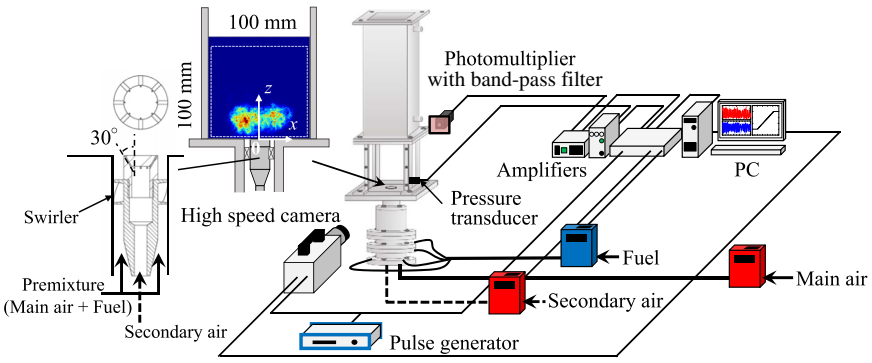

FIG. 1. Schematic of our experimental system.

moment of OH^* chemiluminescence emission intensity fluctuations W'_{OH^*} is defined as $\langle |I'_{OH^*}(x) - \langle I'_{OH^*}(x)\rangle|^2\rangle$, where $\langle\cdot\rangle$ denotes the mean value over I'_{OH^*} with respect to the x direction at a constant z. Similarly to a recent study [12], we set the value of ϵ so as to satisfy $R_r = 0.05$. The phase synchronization parameter quantifying the degree of phase synchronization between p' and W'_{OH^*} is given by

$$r_{pq} = \left| \lim_{\Delta t\to\infty} \frac{1}{\Delta t} \int_t e^{i[\theta_p(t') - \theta_q(t')]} dt' \right|, \tag{3}$$

where Δt is the time interval and $\theta_p(t')$ and $\theta_q(t')$ are the instantaneous phases of p' and W'_{OH^*}, respectively [note that the mathematical formula of Eq. (3) was proposed as the synchronization parameter by Gómez-Gardeñes *et al.* [24]]. r_{pq} is unity (zero) for the in-phase state (antiphase state). An important point is that S_I increases as the mutual coupling between the pressure and heat release rate fluctuations is strengthened.

McCullough *et al.* [25] proposed a transition network taking into account the partition of the time series into symbolic states and the connection between the network nodes based on the transition sequence of symbolic states, referred to as the ordinal partition transition networks. Zhang *et al.* [13] have recently shown the usefulness of the ordinal partition transition networks in the analysis of the interaction patterns between multivariate time series. Kobayashi *et al.* [14] adopted ordinal partition transition networks to study the correlation between two simultaneously measured pressure fluctuations. In this study, we construct the ordinal partition transition networks consisting of order patterns (permutation patterns [26,27]). The order patterns are used as the nodes of the network and the weighted and directed edges are allocated between the nodes on the basis of the transition sequence of order patterns. The weight of an edge is the frequency of the transition route between two order patterns. The ordinal partition transition networks for an m-dimensional time series are expressed by a weighted adjacency matrix $\mathbf{w}$ consisting of $W_{ij} = P(\pi_i \to \pi_j)$, $i,j \in [1, 2^m]$, $\sum_{i,j}^{2^m} W_{ij} = 1$, where P is the existing probability from the ith- to jth-order transition patterns. In this study, the order patterns are π_1, π_2, π_3, and π_4 with the combinations of the signs of the increments taken into consideration for two-dimensional time series $[p'(t), I'_{OH^*}(t)]$.

The SVM [17] searches for an optimal separating hyperplane in the feature space using the given training data set $\{\mathbf{x}_i, y_i\}$, $i = 1, 2, \ldots, n$, where $\mathbf{x}_i$ is the input vector and y_i is the class label taking a value of $+1$ or -1. We first consider Eq. (4) as the optimization problem of the decision function $f(\mathbf{x})[= \boldsymbol{\omega}^T\Phi(\mathbf{x}) + b]$ satisfying $y_i f(\mathbf{x}_i) > 0$:

$$\min_{\boldsymbol{\omega},b,\boldsymbol{\xi}} \frac{1}{2} \parallel \boldsymbol{\omega} \parallel^2 + \gamma \sum_{i\in[n]} \xi_i, \tag{4}$$

such that $-[y_i f(\mathbf{x}_i) - 1 + \xi_i] \le 0$, $\xi_i \ge 0$, $i \in [n]$. Here, ξ_i is the non-negative slack variable corresponding to the margin error and γ is the regularization parameter. In a nonlinear optimization problem, the following Lagrangian function $L(\boldsymbol{\omega}, b, \boldsymbol{\xi}, \mathbf{a}, \boldsymbol{\mu})$ used to treat Eq. (4) and the constraint is defined as

$$L(\boldsymbol{\omega}, b, \boldsymbol{\xi}, \mathbf{a}, \boldsymbol{\mu}) = \frac{1}{2} \parallel \boldsymbol{\omega} \parallel^2 + \gamma \sum_{i\in[n]} \xi_i - \sum_{i\in[n]} a_i[y_i f(\mathbf{x}_i) - 1 + \xi_i] - \sum_{i\in[n]} \mu_i \xi_i. \tag{5}$$

Here, $\mathbf{a}$ $[= (a_1, a_2, \ldots, a_N)^T]$ and $\boldsymbol{\mu}$ $[= (\mu_1, \mu_2, \ldots, \mu_N)^T]$ are the Lagrange multiplier, respectively. Under the stationary condition ($\partial L/\partial\boldsymbol{\omega} = \partial L/\partial b = \partial L/\partial\boldsymbol{\xi} = 0$ and $\mu_i\xi_i = 0$), we obtain the following Lagrangian function in the dual representation $\tilde{L}(\mathbf{a})$:

$$\tilde{L}(\mathbf{a}) = \sum_{i=1}^{N} a_i - \frac{1}{2} \sum_{i=1}^{N} \sum_{j=1}^{N} a_i a_j y_i y_j \Phi(\mathbf{x}_i)^T \Phi(\mathbf{x}_j), \tag{6}$$

such that $0 \le a_i \le \gamma$, $\sum_{i=1}^{N} a_i y_i = 0$. We here consider the radial basis function kernel $k(\mathbf{x}_i, \mathbf{x}_j)$ $[= \exp(-|\mathbf{x}_i - \mathbf{x}_j|^2/2\sigma^2)]$ for $\Phi(\mathbf{x}_i)^T\Phi(\mathbf{x}_j)$. Note that γ and σ are set to 1 and $1/\sqrt{2}$ in this study, respectively. We finally obtain the output of the nonlinear SVM classifier $f(\mathbf{x})$ in Eq. (7) by maximizing Eq. (6):

$$f(\mathbf{x}) = \sum_{i=1}^{N} a_i y_i k(\mathbf{x}, \mathbf{x}_i) + b. \tag{7}$$

The k-means clustering method [17], which allows the distance between noncentral data points and the centroid

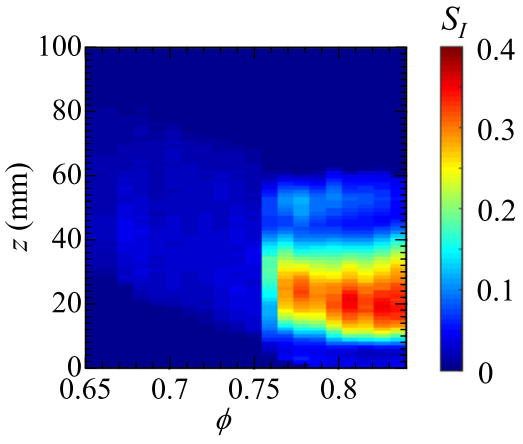

FIG. 2. Variation in the spatial distribution of the synchronization index S_I as a function of equivalence ratio ϕ for different downstream locations z.

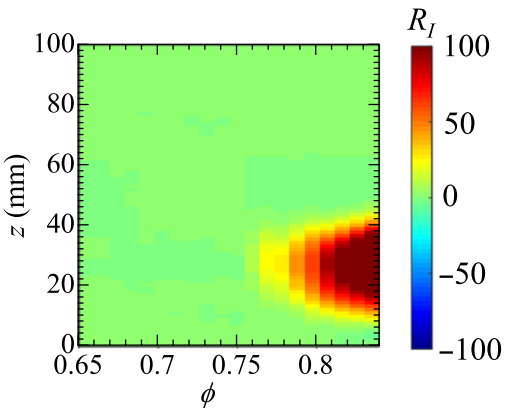

FIG. 3. Variation in the spatial distribution of the Rayleigh index R_I as a function of equivalence ratio ϕ for different downstream locations z.

of each cluster to be minimized, is a well-known partition clustering method of classifying a given data set into k clusters. In this study, we divide samples of training data into three clusters ($k = 3$) using the k-means clustering method. After the class labels of the three clusters are assigned, a SVM classifier is made from the derived cluster centers. Murayama *et al.* [12] showed that a combined methodology of sequential horizontal visibility graph motifs and PCA is useful for capturing a precursor of themoacoustic combustion instability. On this basis, in this study, we apply PCA to the probability distribution in the 16-dimensional transition patterns in ordinal partition transition networks. After obtaining the component scores of the projected probabilities of the transition patterns, we use $\{S_1, S_2\}$ as $\mathbf{x}_i$. Here, S_1 and S_2 are the normalized first and second components in the PCA, respectively.

IV. RESULTS AND DISCUSSION

Figure 2 shows the variation in the spatial distribution of the synchronization index S_I as a function of equivalence ratio ϕ for different downstream locations z. S_I takes a rather low value at $\phi = 0.67$ corresponding to the formation regime of combustion noise, and remains almost unchanged at $\phi \leq 0.75$. As ϕ exceeds approximately 0.76, S_I starts to significantly increase in the range of $15 \leq z \leq 38$ mm owing to the onset of thermoacoustic combustion instability. This clearly shows that a synchronized state [18] due to significant positive coupling between pressure and heat-release-rate fluctuations emerges in the region from near the flame base to the shear layer between the two dominant large-scale recirculation flows: the inner recirculation flow above the centerbody and the outer recirculation flow in the dump corner of the combustor [12]. An important point to emphasize regarding Fig. 2 is the high S_I near the flame base subjected to noisy periodic oscillations [12] in flow velocity field. On this basis, as will be shown later in Fig. 6, we inject a strong secondary air jet to the oscillating flame base causing a significant change in the convective vortical structures so as to prevent the formation of the synchronized state.

The Rayleigh index is a well-recognized important measure for quantifying the interaction between pressure and heat-release-rate fluctuations during thermoacoustic combustion oscillations. We here compare the spatial distributions of S_I and the Rayleigh index R_I to show the applicability of S_I. The spatial distribution of R_I is shown in Fig. 3 as a function of ϕ. The distribution of S_I reasonably corresponds to that of R_I, appropriately capturing the driving regime of thermoacoustic combustion oscillations. The important point to note here is that S_I captures the precursor of thermoacoustic combustion oscillations at $\phi \sim 0.75$, whereas R_I begins to significantly change at $\phi \sim 0.77$. This means that the synchronization index is more suitable for detecting the precursor of thermoacoustic

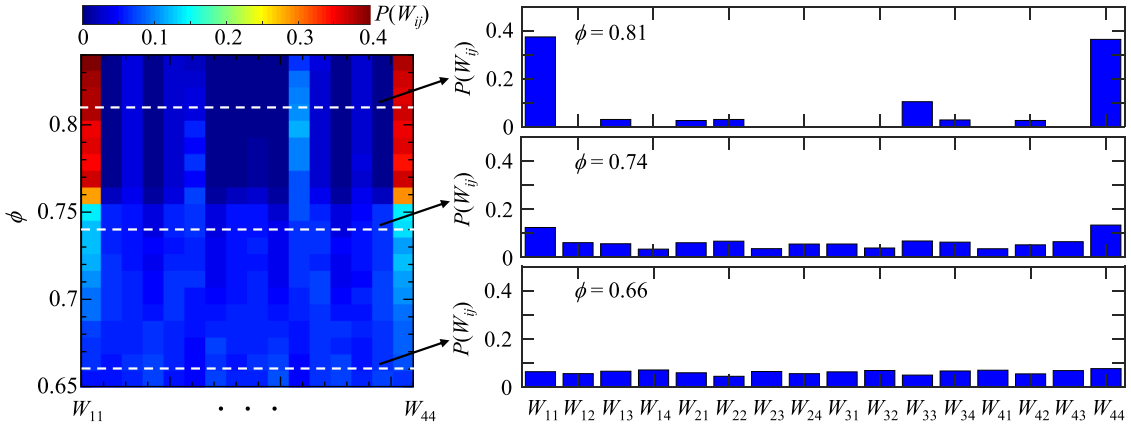

FIG. 4. Variation in the probability distribution of the transition patterns in the ordinal partition transition networks $P(W_{ij})$ as a function of equivalence ratio ϕ.

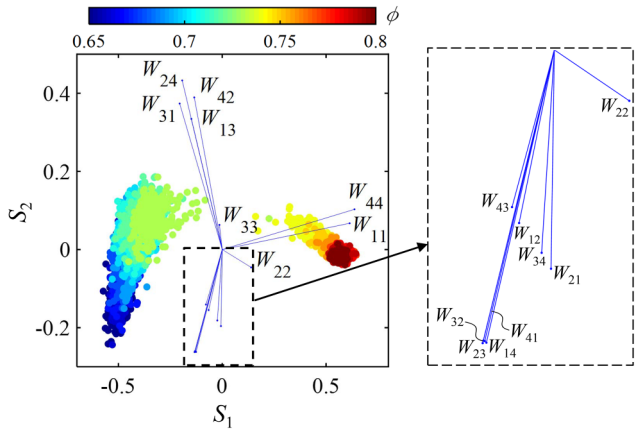

FIG. 5. Passage on the S_1-S_2 plane obtained from PCA of the probability distribution of the transition patterns in ordinal partition transition networks in terms of the equivalence ratio ϕ. Here, S_1 and S_2 are the first and second components, respectively, and the blue lines W_{ij} on the S_1-S_2 plane represent the embedded manifold coordinates in 16 dimensions.

combustion oscillations than the Rayleigh index. In addition, the synchronization index enables us to quantify the degree of interaction between pressure and heat-release-rate fluctuations in the range from zero to unity. In contrast, the Rayleigh index is sensitive to the amplitudes of pressure and heat-release-rate fluctuations and does not range from zero to unity. In these contexts, the synchronization index is better suited for the treatment of the interaction between pressure and heat-release-rate fluctuations than the Rayleigh index.

Figure 4 shows the probability distribution of the transition patterns from the ith to jth order in the ordinal partition transition networks $P(W_{ij})$ as a function of ϕ. We observe an almost uniform probability distribution at $\phi \leq 0.70$. This means that all the transition patterns randomly occur during combustion noise. As thermoacoustic combustion instability is induced with increasing ϕ, two peaks notably begin to appear at $W_{11}(\pi_1 \rightarrow \pi_1)$ and $W_{44}(\pi_4 \rightarrow \pi_4)$ with some other peaks, which correspond to monotonically increasing and decreasing processes [13] of both pressure and heat-release-rate fluctuations. They become predominant during well-developed thermoacoustic combustion instability, which clearly shows the significant formation of an in-phase state between pressure and heat-release-rate fluctuations. Ordinal partition transition networks are valid for capturing the inception of the in-phase state associated with the onset of thermoacoustic combustion instability. The passage on the S_1-S_2 plane obtained by PCA is shown in Fig. 5 in terms of ϕ, where S_1 (S_2) is the first (second) component. The location of (S_1, S_2) moves from left to right on the S_1-S_2 plane with increasing ϕ, forming a distribution with a paraboliclike shape. This result shows that the principal component plane of the probability distribution of the transition patterns sufficiently captures the significant transition from combustion noise to well-developed thermoacoustic combustion instability with increasing equivalence ratio. Figure 6(A) shows the feature space consisting of S_1 and S_2 obtained by the SVM. The SVM allows the combustion state to be clearly classified into three regimes on the feature space: combustion noise (blue), thermoacoustic combustion instability (red), and the transition from combustion noise to thermoacoustic combustion instability (yellow). As shown in Fig. 6(B), we here gradually increase ϕ with time so as to induce well-developed thermoacoustic combustion instability. The black plots corresponding to p' and I'_{OH^*} are drawn on the S_1-S_2 plane with increasing time. An important point is that the combustion state switches back and forth between combustion noise and the transition at approximately $16 \leq t \leq 29$ s and finally leads to thermoacoustic combustion instability at approximately $t = 30$ s. This demonstrates that the feature space captures the significant transition from combustion noise to thermoacoustic combustion instability.

The prevention and suppression of thermoacoustic combustion instability by using the feature space are attempted online in this study with the aim of examining their

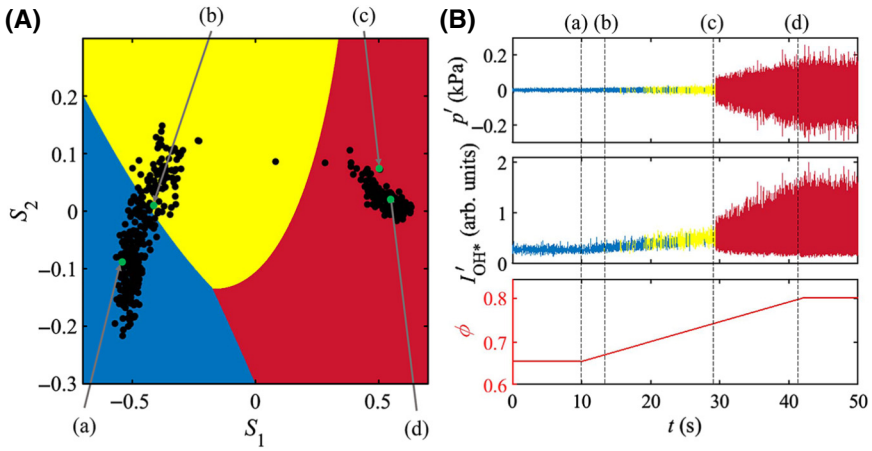

FIG. 6. (A) The feature space consisting of the first component S_1 and second component S_2 obtained by SVM. (B) Time variations in pressure fluctuations p' and OH* chemiluminescence emission intensity fluctuations I'_{OH^*} with increasing equivalence ratio ϕ. (a) $t = 10.0$ s, (b) $t = 13.4$ s, (c) $t = 29.6$ s, and (d) $t = 42.0$ s.

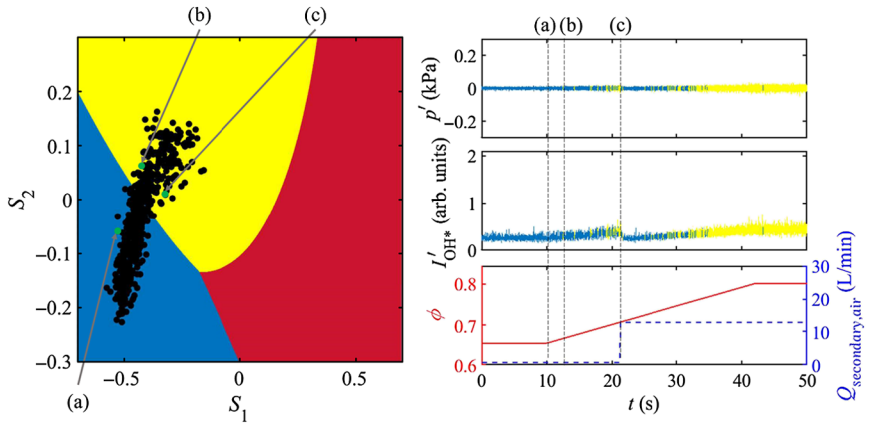

FIG. 7. Time variations in pressure fluctuations p' and OH^* chemiluminescence emission intensity fluctuations I'_{OH^*} with increasing equivalence ratio ϕ, together with the feature space. (a) $t = 10.0$ s, (b) $t = 12.6$ s, and (c) $t = 21.3$ s. Note that a secondary air injection is issued from the injector rim shortly after detecting a precursor of thermoacoustic combustion instability.

potential practical applications. We define the transition state percentage R_t as the ratio of the formation duration of the transition state to that of the combustion noise state and compute it every 100 ms. A secondary air jet from the injector (see Fig. 1) is added to the flame base when R_t exceeds 50% with increasing time. Note that we set the steady air percentage (SAP) [$= Q_{secondary,air}/Q_{main,air}$, where $Q_{secondary,air}$ ($Q_{main,air}$) is the secondary (main) air flow rate] to 8.5% to sufficiently suppress thermoacoustic combustion instability [18]. Time variations in p' and I'_{OH^*} with increasing ϕ are shown in Fig. 7, together with the feature space. ϕ is gradually increased until thermoacoustic combustion instability occurs, but both p' and I'_{OH^*} are successfully controlled by the addition of a secondary air jet from the injector rim shortly after detecting a precursor of thermoacoustic combustion instability at $t = 21.3$ s. This result indicates that the prevention and suppression of thermoacoustic combustion instability are feasible without knowing its actual onset. Our group has recently presented two measures for detecting a precursor of thermoacoustic combustion instability: a modified version of the permutation entropy [28] and the first-principals component in the probability distribution of the motif patterns in the sequential horizontal visibility graph [12]. Other groups have also recently presented the importance of measures such as the Hurst exponent in the singularity spectrum [29,30] and the recurrence rate in the recurrence plots [31], which make it possible to detect the onset of thermoacoustic combustion instability. Note that in these studies [12,28–31], pressure fluctuation data were used to estimate the measures. The proposed combinational methodology of ordinal transition partition networks, PCA, and a SVM using k-means clustering, which considers the mutual coupling between pressure and heat-release-rate fluctuations, has considerable potential for the early detection of thermoacoustic combustion instability. A complex-networks/machine-learning-based approach for the early detection of thermoacoustic combustion instability has not been adopted in previous studies on thermoacoustic systems. Two recent experimental studies have dealt with the transition during thermoacoustic combustion oscillations: a model aircraft engine staging combustor [28] and a model rocket engine combustor [32]. In the former, the amount of the main fuel was gradually changed with time, whereas in the latter, the amount of nitrogen was similarly changed to transiently induce thermoacoustic combustion oscillations. In this study, we dealt with a swirl-stabilized turbulent combustor, focusing on the two representative experimental conditions. We need to examine the applicability of our methodologies to different combustors in future studies.

V. SUMMARY

We have conducted an experimental study on the early detection of combustion-driven thermoacoustic instability using a combinational methodology of complex networks and machine learning. We use ordinal partition transition networks considering the mutual interaction between pressure and heat-release-rate fluctuations inside a swirl-stabilized turbulent combustor. The probability distribution of the transition patterns in ordinal partition transition networks significantly captures the subtle changes in the combustion state during a transition from combustion noise with a low amplitude to thermoacoustic combustion instability with a large amplitude, identifying the inception of the in-phase state associated with the onset of thermoacoustic combustion instability. A two-dimensional feature space consisting of the first and second components estimated from the probability distribution in the transition patterns, which is obtained by a support vector machine using k-means clustering, allows us to detect a precursor of thermoacoustic combustion instability. The combustion state is successfully controlled shortly after detecting a precursor of thermoacoustic combustion instability by the support vector machine.

ACKNOWLEDGMENTS

H.G. is supported by a Grant-in-Aid for Scientific Research (B) No. 19H02085 and the Suzuki Foundation.

We thank Mr. Hayato Todoroki (Photron Co.) for helping us use the high-speed video camera (Photron, FASTCAM SA-Z) employed in this study. We would like to express our thanks to Souta Nakano, Shinga Masuda, and Takuya Kurosaka (Tokyo University of Science) for their support of our experiments.

[1] T. Biwa, Y. Tashiro, M. Ishigaki, Y. Ueda, and T. Yazaki, Measurements of acoustic streaming in a looped-tube thermoacoustic engine with a jet pump, J. Appl. Phys. **101**, 064914 (2007).

[2] T. Biwa, D. Hasegawa, and T. Yazaki, Low temperature differential thermoacoustic Stirling engine, Appl. Phys. Lett. **97**, 034102 (2010).

[3] Y. Huang and V. Yang, Dynamics and stability of lean-premixed swirl-stabilized combustion, Prog. Energy Combust. Sci. **35**, 293 (2009).

[4] T. C. Lieuwen, *Unsteady Combustor Physics* (Cambridge University Press, Cambridge, 2012).

[5] M. P. Juniper and R. I. Sujith, Sensitivity and nonlinearity of thermoacoustic oscillations, Annu. Rev. Fluid Mech. **50**, 661 (2018).

[6] T. Biwa, S. Tozuka, and T. Yazaki, Amplitude Death in Coupled Thermoacoustic Oscillators, Phys. Rev. Appl. **3**, 034006 (2015).

[7] M. E. J. Newman, *Networks: An Introduction* (Oxford University Press, Oxford, 2010).

[8] M. Murugesan and R. I. Sujith, Combustion noise is scale-free: transition from scale-free to order at the onset of thermoacoustic instability, J. Fluid Mech. **772**, 225 (2015).

[9] M. Murugesan and R. I. Sujith, Detecting the onset of an impending thermoacoustic instability using complex networks, J. Propul. Power **32**, 707 (2016).

[10] H. Gotoda, H. Kinugawa, R. Tsujimoto, S. Domen, and Y. Okuno, Characterization of Combustion Dynamics, Detection, and Prevention of an Unstable Combustion State Based on a Complex-Network Theory, Phys. Rev. Appl. **7**, 044027 (2017).

[11] Y. Okuno, M. Small, and H. Gotoda, Dynamics of self-excited thermoacoustic instability in a combustion system: Pseudo periodic and high-dimensional nature, Chaos **25**, 043107 (2015).

[12] S. Murayama, H. Kinugawa, I. T. Tokuda, and H. Gotoda, Characterization and detection of thermoacoustic combustion oscillations based on statistical complexity and complex-network theory, Phys. Rev. E **97**, 022223 (2018).

[13] J. Zhang, J. Zhou, M. Tang, H. Guo, M. Small, and Y. Zou, Constructing ordinal partition transition networks from multivariate time series, Sci. Rep. **7**, 7795 (2017).

[14] H. Kobayashi, H. Gotoda, and S. Tachibana, Nonlinear determinism in degenerated combustion instability in a gas-turbine model combustor, Physica A **510**, 345 (2018).

[15] V. N. Vapnik, *The Nature of Statistical Learning Theory* (Springer-Verlag, New York, 1995).

[16] V. N. Vapnik, An overview of statistical learning theory, IEEE Trans. Neural Netw. **10**, 988 (1999).

[17] C. M. Bishop, *Pattern Recognition and Machine Learning* (Springer-Verlag, New York, 2006).

[18] S. Murayama and H. Gotoda, Attenuation behavior of thermoacoustic combustion instability analyzed by complex-network- and synchronization-based approach, Phys. Rev. E **99**, 052222 (2019).

[19] S. Mondal, V. R. Unni, and R. I. Sujith, Onset of thermoacoustic instability in turbulent combustors: an emergence of synchronized periodicity through formation of chimera-like states, J. Fluid Mech. **811**, 659 (2017).

[20] N. B. George, V. R. Unni, M. Raghunathan, and R. I. Sujith, Pattern formation during transition from combustion noise to thermoacoustic instability via intermittency, J. Fluid Mech. **849**, 615 (2018).

[21] V. Godavarthi, S. A. Pawar, V. R. Unni, R. I. Sujith, N. Marwan, and J. Kurths, Coupled interaction between unsteady flame dynamics and acoustic field in a turbulent combustor, Chaos **28**, 113111 (2018).

[22] Y. Guan, M. Murugesan, and L. K. B. Li, Strange nonchaotic and chaotic attractors in a self-excited thermoacoustic oscillator subjected to external periodic forcing, Chaos **28**, 093109 (2018).

[23] N. Marwan, M. C. Romano, M. Thiel, and J. Kurths, Recurrence plots for the analysis of complex systems, Phys. Rep. **438**, 237 (2007).

[24] J. Gómez-Gardeñes, Y. Moreno, and A. Arenas, Paths to Synchronization on Complex Networks, Phys. Rev. Lett. **98**, 034101 (2007).

[25] M. McCullough, M. Small, T. Stemler, and H. Ho-Ching Iu, Time lagged ordinal partition networks for capturing dynamics of continuous dynamical systems, Chaos **25**, 053101 (2015).

[26] C. Bandt and B. Pompe, Permutation Entropy: A Natural Complexity Measure for Time Series, Phys. Rev. Lett. **88**, 174102 (2002).

[27] C. W. Kulp and L. Zunino, Discriminating chaotic and stochastic dynamics through the permutation spectrum test, Chaos **24**, 033116 (2014).

[28] H. Kobayashi, H. Gotoda, S. Tachibana, and S. Yoshida, Detection of frequency-mode-shift during thermoacoustic combustion oscillations in a staged aircraft engine model combustor, J. Appl. Phys. **122**, 224904 (2017).

[29] V. Nair and R. I. Sujith, Multifractality in combustion noise: predicting an impending combustion instability, J. Fluid Mech. **747**, 635 (2014).

[30] V. Nair, G. Thampi, and R. I. Sujith, Intermittency route to thermoacoustic instability in turbulent combustors, J. Fluid Mech. **756**, 470 (2014).

[31] V. R. Unni and R. I. Sujith, Multifractal characteristics of combustor dynamics close to lean blowout, J. Fluid Mech. **784**, 30 (2015).

[32] H. Kasuya, H. Gotoda, S. Yoshida, and S. Tachibana, Dynamic behavior of combustion instability in a cylindrical combustor with an off-center installed coaxial injector, Chaos **28**, 033111 (2018).